Experimental Mass Transfer at a Forced-Convective Rotating-Disk Electrode

Shi-Chern Yen* and Jin-Shen Wang

Department of Chemical Engineering, National Taiwan University, Taipei, Taiwan 106, China

Thomas W. Chapman*

Department of Chemical Engineering, University of Wisconsin, Madison, Madison, Wisconsin 53706

ABSTRACT

The mass transfer at a rotating-disk electrode with an external forced convection has been studied in this paper. The mass-transfer factor of the forced-convective rotating disk suitable for Schmidt numbers greater than 1 is presented. The limiting currents of the ferricyanide reduction at various forced-flow strength and rotating speeds were measured experimentally and used to estimate the mass transfer at the forced-convective rotating disk. It is found that the experimental results agree very well with the values calculated theoretically.

The fluid flow and mass transfer (or heat transfer) near a rotating disk in the presence of an external forced flow is an interesting problem worthy of investigation. There are two limiting cases of this flow type. One is the flow induced by a rotating disk, which is well known in electrochemistry, and the other is the axisymmetrical flow with stagnation on a planar wall. Both have been applied extensively in many fields[1-4].

The solution of fluid flow induced purely by a rotating disk was first obtained by von Kármán[5] and later by Cochran[6]. The works of von Kármán and Cochran have stimulated numerous authors to study fluid flow near a rotating disk by using various methods. The relevant heat or mass transfer to a rotating disk has been studied extensively. The asymptote derived by Levich[1] is suitable for high Schmidt numbers. Corrections to this asymptote were presented by Sparrow and Gregg[7], Newman[8], and Liu and Stewart[9], respectively, so they can be applied to moderate and low Schmidt numbers. Generally, the experimental data were found to have good agreement with the theoretical values for laminar flow[10-13]. As for transition ($3 \times 10^5 < Re < 10^6$) and turbulent flows ($Re > 10^6$), most of the studies were experimental approach and correlations applied to various regions of Reynolds numbers are available in the literature[12,14,15].

On the other hand, the impinging jet on a flat plate is also an interesting flow which can provide "uniform accessibility" at its center spot for heat or mass transfer similar to that on a rotating disk. Because of this property it receives the same attention as the rotating disk. From the results in the literature[4,16-19], it is concluded that the local transfer rate depends on the Reynolds number of the fluid in the nozzle, the Schmidt number of the diffusing species, the nozzle height, and the radial position on the plate. The dependences on these parameters are somewhat different in the stagnation and wall-jet regions on the impinged plane[4,16-19]. The flow pattern in the nozzle also plays an important role in heat or mass transfer of an impinging jet. Scholtz and Trass[16] considered an impinging jet with a parabolic velocity distribution. In addition to the theoretical and experimental examinations of fluid flow, the local mass-transfer coefficients have been calculated theoretically and compared with the experimental data for the air-naphthalene system. It was pointed out that even at equal Reynolds numbers, the mass transfer observed for a nonuniform jet at the stagnation point is two times that calculated for a uniform jet. Recently several investigators utilized the impinging jet system for electrochemical studies[18-22]. Chin and Tsang[20] presented both the theoretical and experimental studies of mass transfer at a circular disk electrode in the stagnation region of an impinging jet. Part of their theoretical analysis was essentially a limiting case of this study. Chin and Chandran[21] extended the study to a ring disk electrode and tried to develop the impinging jet as a practical tool for electroanalytical applications. Alkire and Chen[22] utilized an unsubmerged jet system to study high-speed selective electroplating. Mass-transfer measurements were carried out in the impingement zone by using disk electrodes of different radii and in the wall-jet region by using a sectioned electrode, respectively. As for the mass transfer in the impingement zone, the experimental data were within 10% of the correlation presented by Chin and Tsang[20].

As for the fluid flow and mass transfer of a rotating disk coupled with an external forced convection, Hannah[23] first gave the solution for the forced-convective rotating disk by expressing the velocity profiles near the disk surface in power series which were similar to those by Cochran[6]. There were some flow constants to be determined, and these constants were obtained numerically through a tedious procedure of trial and integration. Afterwards, Schlichting and Truckenbrodt[24] obtained an approximate solution by using the integral method and assuming the velocity components in the radial and azimuthal directions as polynomials of the dimensionless distance from the wall, which fulfill the constrained boundary conditions at the wall and at the edge of the boundary layer. The relevant heat-transfer problem in this flow field was solved numerically by Tien and Tsuji[25]. Hannah's velocity functions were used to obtain the temperature profile. Besides the numerical calculations for moderate Prandtl numbers, asymptotic heat-transfer relations for large and small Prandtl numbers were also given. Recently, Lee *et al.*[26] extended the problem to the more general case of heat transfer over rotating bodies. The momentum- and heat-transfer rates were calculated numerically by employing Merk's series-expansion technique. Koong and Blackshear[27] computed the average Nusselt number for the rotating disk in approach flow by measuring the mass-transfer rates of naphthalene sublimation in air (Sc = 2.4). They found that the experimentally measured Nusselt numbers agreed with the theoretical results modified from the correlation of Schlichting and Truckenbrodt[24].

In this paper, the velocity field will be estimated from the Navier-Stokes equation, and the flow constants pertinent to the expanded series will be presented as functions of the dimensionless flow constant of the external forced flow. The corresponding mass-transfer correlation which is value for $Sc > 1$ is also formulated. To confirm the theoretical analysis, we also utilize an electrochemical method to measure the mass-transfer rates at the forced-convective rotating disk. Electrochemical measurement is convenient and avoids the problems such as surface roughness and simultaneous heat transfer which arises in measuring mass-transfer rates by sublimation from a solid surface. This study also lays the foundation for analyzing the mass

* Electrochemical Society Active Member.

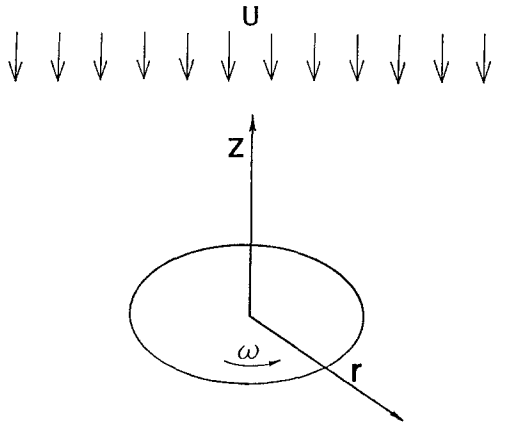

Fig. 1. The rotating disk in a uniform flow field with the uniform approaching velocity *U*.

transfer of a two-phase flow system at a rotating disk with an external forced convection.

Theoretical

The flow system considered here is a uniform, normal, laminar forced flow of an incompressible fluid against a rotating disk of infinite radius as indicated in Fig. 1. If the flow is axially symmetrical, under steady state, the governing Navier-Stokes equation may be reduced to a set of ordinary differential equations by introducing the following variables[23]

$$u = \lambda r F(\zeta) \quad v = \omega r G(\zeta) \quad w = (\nu\lambda)^{1/2} H(\zeta) \qquad [1]$$

and

$$\lambda = (k^2 + \omega^2)^{1/2} \quad \zeta = (\lambda/\nu)^{1/2} z \qquad [2]$$

where ζ is a dimensionless distance from the disk surface, and k is a hydrodynamic constant which indicates the intensity of the forced flow. The definition of k will be related to the free-stream velocity U in a later section (see Eq. 26). Other variables are defined in the list of symbols. The equations of continuity and motion become

continuity

$$H' + 2F = 0 \qquad [3]$$

motion

$$F''' - HF'' = F^2 - \Omega^2 G^2 - K^2 \qquad [4]$$

$$G'' - HG' - 2FG = 0 \qquad [5]$$

The boundary conditions after the above transformation are

at

$$\zeta = 0 \quad F = H = 0 \quad G = 1 \qquad [6]$$

and

at

$$\zeta \to \infty \quad F = K \quad G = 0 \qquad [7]$$

where $\Omega = \omega/\lambda$, $K = k/\lambda$, and $\Omega^2 + K^2 = 1$. For very large ζ (far from the surface), H will approach

$$H \sim -2K\zeta - C \qquad [8]$$

where C is a flow constant which needs to be determined in the numerical computation to satisfy Eq. 3-5

The dimensionless velocities, F, G, H can be expanded for small ζ in series form as

$$F(\zeta) = a\zeta - \frac{1}{2}\zeta^2 - \frac{1}{3}b\Omega^2\zeta^3 - \frac{1}{12}b^2\Omega^2\zeta^4 + \ldots \qquad [9]$$

$$G(\zeta) = 1 + b\zeta + \frac{1}{3}a\zeta^3 + \frac{1}{12}(ab - 1)\zeta^4 + \ldots \qquad [10]$$

Table I. Values of *a*, *b*, and *C* at various μ (=Ω/*K*).

μ (*K*)	∞ (0.00000)	2 (0.44721)	1 (0.70711)	1/2 (0.89443)	0 (1.00000)
a	0.51024	0.68655	0.93586	1.16627	1.31194
b	−0.61593	−0.80039	−0.93339	−1.02510	−1.07467
C	0.88448	−0.55216	−0.87984	−1.05335	−1.13780

$$H(\zeta) = -a\zeta^2 + \frac{1}{3}\zeta^3 + \frac{1}{6}b\Omega^2\zeta^4 + \frac{1}{30}b^2\Omega^2\zeta^5 + \frac{1}{180}a(\Omega^2 - K^2)\zeta^6 + \ldots \qquad [11]$$

Yen and Wang[29] computed the velocities by the method of orthogonal collocation suggested by Caban and Chapman[29]. The results were summarized in Table I. Values of a, b, and C were correlated by the dimensionless hydrodynamic constant K and expressed in a polynomial form as

$$a = 0.51023 - 0.03247K + 1.04818K^2 - 0.21397K^3 \qquad [12]$$

$$b = -0.61592 - 0.17712K - 0.90859K^2 + 1.02633K^3 - 0.40094K^4 \qquad [13]$$

$$C = 0.88447 - 7.17826K + 20.63814K^2 - 49.48305K^3 + 74.03479K^4 - 58.13316K^5 + 18.10503K^6 \qquad [14]$$

The above equations are handy in calculating a, b, and C for various values of the dimensionless forced-flow constant K; the standard deviations are 0.00098 for a, 0.00087 for b, and 0.0042 for C, respectively.

If the disk is infinitely large and the interfacial concentration is uniform, the concentration profile is independent of the r and θ directions, and the convective diffusion equation in dimensionless form at steady state becomes

$$\Theta'' - \mathrm{Sc}H\Theta' = 0 \qquad [15]$$

with the boundary conditions

at

$$\zeta = 0 \quad \Theta = 0 \qquad [16]$$

at

$$\zeta \to \infty \quad \Theta = 1$$

where Sc is the Schmidt number, ν/D_i, and Θ represents the dimensionless concentration. The Sherwood number for mass transfer is expressed as

$$\mathrm{Sh} \equiv \frac{k_m}{D_i}\left(\frac{\lambda}{\nu}\right)^{-1/2} = \Theta'(0) \qquad [17]$$

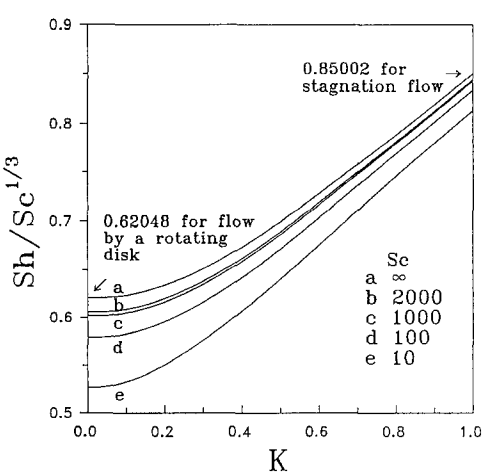

Fig. 2. Dimensionless mass-transfer factor *vs.* the dimensionless hydrodynamic strength for a rotating disk with an external forced flow at various Schmidt numbers.

Table II. Comparison of the asymptotic value with the complete solution of the dimensionless mass-transfer factor for Sc ≥ 1.

	$ShSc^{-1/3}$							
	μ = 0 (K = 1.000)		μ = 1 (K = 0.707)		μ = 2 (K = 0.894)		μ = ∞ (K = 0.000)	
Sc	Eq. 19	Complete	Eq. 19	Complete	Eq. 19	Complete	Eq. 19	Complete
1000	0.8427	0.8427	0.7494	0.7494	0.6713	0.6713	0.6016	0.6016
100	0.8338	0.8338	0.7378	0.7378	0.6555	0.6555	0.5789	0.5789
10	0.8132	0.8133	0.7127	0.7126	0.6225	0.6223	0.5266	0.5264
5	0.8024	0.8025	0.7004	0.7003	0.6071	0.6069	0.4995	0.4990
2	0.7823	0.7828	0.6790	0.6791	0.5821	0.5814	0.4506	0.4486
1	0.7607	0.7622	0.6575	0.6582	0.5596	0.5577	0.4007	0.3963

where Sh involves λ to provide the characteristic length. Θ'(0) can be obtained by integrating Eq. 22 with the given boundary conditions as

$$\Theta'(0) = \frac{1}{\int_0^\infty \exp\left\{\mathrm{Sc}\int_0^\zeta H(\zeta_1)d\zeta_1\right\}d\zeta} \quad [18]$$

The complete solution for Sherwood number was found by numerical integration. The resulting dimensionless mass-transfer factor $Sh/Sc^{1/3}$ as a function of the forced-flow strength K at various Schmidt numbers is shown in Fig. 2.

Asymptotic solution of mass transfer.—Equation 11 is substituted into Eq. 18, and part of the integrand in Eq. 18 is expanded in power series of Sc, the Sherwood number is formulated as[9,28,30]

$$\mathrm{Sh} = \frac{\mathrm{Sc}^{1/3}}{f_1 + f_2\mathrm{Sc}^{-1/3} + f_3\mathrm{Sc}^{-2/3} + f_4\mathrm{Sc}^{-1} + f_5\mathrm{Sc}^{-4/3} + \ldots} \quad [19]$$

where

$$f_1 = \frac{1}{3}g_1\Gamma\left(\frac{1}{3}\right) = \frac{1}{3}\left(\frac{3}{a}\right)^{1/3}\Gamma\left(\frac{1}{3}\right)$$

$$f_2 = \frac{2}{9}g_1g_2\Gamma\left(\frac{2}{3}\right) = \frac{1}{54}\left(\frac{3}{a}\right)^{5/3}\Gamma\left(\frac{2}{3}\right)$$

$$f_3 = \frac{1}{3}g_1(g_3 + g_2^2)$$

$$f_4 = \frac{1}{729}g_1(108g_4 + 252g_2g_3 + 140g_2^3)\Gamma\left(\frac{1}{3}\right)$$

$$f_5 = \frac{1}{2187}g_1[810g_5 + 1080(g_3^2 + 2g_2g_4) + 3960g_2^2g_3 + 1540g_2^4]\Gamma\left(\frac{2}{3}\right) \quad [20]$$

and

$$g_1 = \left(\frac{3}{a}\right)^{1/3} \quad g_2 = \frac{1}{12}\left(\frac{3}{a}\right)^{4/3} \quad g_3 = \frac{1}{30}b\Omega^2\left(\frac{3}{a}\right)^{5/3}$$

$$g_4 = \frac{1}{180}b^2\Omega^2\left(\frac{3}{a}\right)^2 \quad g_5 = \frac{1}{1260}a(\Omega^2 - K^2)\left(\frac{3}{a}\right)^{7/3} \quad [21]$$

Thus, the values of f_i and g_i can be estimated for any set of flow constants a and b, which depend on the forced-flow strength K and are estimated according to Eq. 12-14 or the numerical computation.

The dimensionless mass-transfer factor $Sh/Sc^{1/3}$ calculated by Eq. 19 and the complete solution are listed in Table II. The complete solution is computed directly from Eq. 18. It is shown that the values predicted by the asymptotic formula, Eq.19 can be valid down to Sc = 1. If the Schmidt number is large enough, the velocity function in the concentration boundary layer may be approximated as $-a\zeta^2$, and Eq. 19 may be further simplified as

$$\frac{\mathrm{Sh}}{\mathrm{Sc}^{1/3}} = 0.7765a^{1/3} \quad [22]$$

For the flow induced purely by a rotating disk, $Sh/Sc^{1/3}$ is 0.62048 calculated with a = 0.51023 and the above equation, which shows good agreement with the ones presented in the cited literature[31]. Practically, the Schmidt number is on the order of 1000 for diffusion in liquids, and Eq. 22 overestimates the mass transfer even at Sc = 1000. The error at Sc = 1000 is about 3% for the pure rotating-disk flow (K = 0) and 0.9% for the axisymmetrical stagnation flow (K = 1).

Experimental

Although the rotating disks used in the experiment were finite, the radii of the disks were considered very large when compared with the boundary-layer thickness of velocity or concentration. The flow can be treated as that caused by an infinite disk. Similarly, the radial diffusion is usually neglected due to the thinness of the diffusion layer compared with the radius of the electrode[32]. In addition, the side wall of the electrolytic cell was set five times larger than the diameter of the disk to avoid the effect from enclosure geometry. In order to match the conditions considered in the theoretical analysis, we employed a rotating disk of which the radius (r_o = 0.666 cm) was smaller than the radius of the nozzle (r_n = 0.8 cm). The relative size of nozzle to disk makes the experimental condition closer to a uniform flow approaching to a finite disk so that the value of flow constant k can be determined. For comparison, we also employed another rotating disk of which the radius (r_o = 0.9 cm) was larger than that of the nozzle. This electrode geometry is usually used in the investigation of impinging jet electrode. The determination of the hydrodynamic strength k depends on the geometry of the nozzle, the dimensionless nozzle height, and the exit flow condition, so a number of correlations are available[20]. Besides the two different disks were used in the measurements, the effect of the nozzle height on the mass-transfer rates was also demonstrated in our experiments.

The electrolyte was composed of 2 mM potassium ferricyanide, 2 mM potassium ferrocyanide, and 0.2M sodium sulfate. The viscosity and density of the solution at 25°C were determined to be 0.963 cp and 1.028 g/cm^3, respectively. Analytical grade chemicals (Merck Co.) and doubly distilled water were used throughout. The temperature in all experiments was controlled at 25 ± 0.1°C. Nitrogen gas was bubbled through the solution for at least 2 h before each experiment and kept passing over it during the run.

The working electrode was a platinum disk of 0.457 cm in diameter embedded in a Teflon rod either 1.333 or 1.8 cm in diameter. The electrode was first polished with 0.05 μm alumina on a microcloth (Ecomet, Buehler) to a mirror-like finish. Then, it was treated electrochemically in 0.5M H_2SO_4 according to the method suggested by Gileadi *et al.*[33]. The potential was set at 1.8 V *vs.* SCE for 10 s to oxidize impurities on the electrode surface and changed to 1.2 V for 30 s to remove oxygen formed at the higher potential. Then the oxides formed at the electrode surface in the previous steps were reduced cathodically by setting the potential at 0.05 V. This procedure was repeated five times.

In our experiments, the reduction of ferricyanide ion at the working electrode was used for limiting-current measurements. The current was obtained by scanning the potential from 0.3 V to −0.4 V *vs.* SCE with a scan rate 5 mV/s in the negative direction, which yielded current plateaus almost identical to the current obtained at the fixed potential

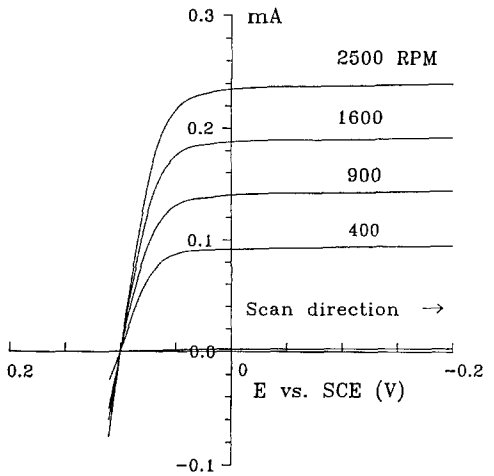

Fig. 3. Voltammograms at rotating-disk electrode for the reduction of $Fe(CN)_6^{-3}$.

−0.3 V. An X-Y recorder (Yew 3086) was connected to the potentiostat/galvanostat (PAR Model 273) to record the current-voltage curves. The experimental results of the polarization curves are shown in Fig. 3. As the applied voltage is increased, the current is first increased, and then leveled off to form a plateau. There seemed to be a slight upward slope for these polarization curves under various rotating speeds. It was attributed to the background current generated during scan as can be indicated in the polarization curve of 0.2*M* Na_2SO_4 blank solution. However, the background current was so small that the current plateaus could be taken as the limiting current for the reduction of ferricyanide. The diffusion coefficient of ferricyanide ion can be obtained from the relation between limiting currents and rotating speeds.

The experimental setup used to determine the mass-transfer coefficient k_m is shown in Fig. 4. Where there were

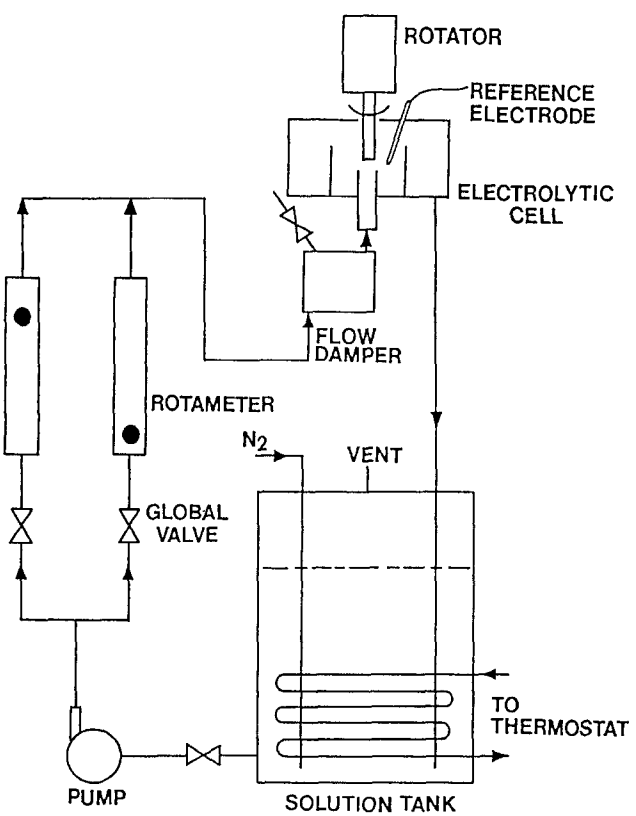

Fig. 4. The experimental setup for mass transfer at the forced-convective rotating-disk electrode.

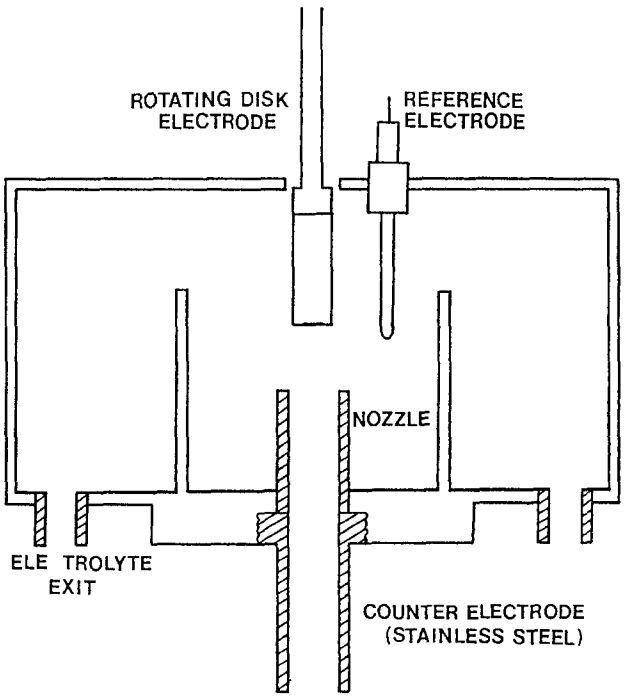

Fig. 5. The configuration of the electrolytic cell.

two rotameters, one was used for flow rates between 0.5 and 4 liter/min, and the other was used for flow rates greater than 4 liter/min. A flow damper downstream of the rotameters was used to eliminate any disturbance in the electrolyte flow rate and to make the velocity profile more uniform before it entered into the impinging jet. In the electrolytic cell (see Fig. 5), an acrylic tube with an inside diameter of 16 mm located in the center of the bottom plate was used as a nozzle, and the nozzle-disk distance was 15 mm. A stainless-steel tube of the same diameter (7 cm in length) screwed to the acrylic tube served as counterelectrode. The limiting currents were measured by setting the potential at −0.3 V *vs.* SCE. At this applied voltage, it has been ascertained that all the currents were under mass-transfer control in our experimental ranges. The current was measured for each flow rate at several rotation speeds. The currents were sampled at a rate of 0.01 s per sampling point, and the average value of one hundred samples was taken as one data point for current. From the relation between the limiting current density and the ion flux, the mass-transfer coefficient can be easily calculated, *i.e.*

$$k_m = \frac{i_l}{nFC_{i,b}} \qquad [23]$$

The limiting currents used for the determination of the mass-transfer coefficient k_m were found to fluctuate during the measurements. The fluctuation was small when the flow in the nozzle was laminar and became more obvious when the flow was turbulent. In general, it was about 2% of the average limiting current. The limiting currents were averaged to give a value for calculation of the mass-transfer coefficient.

Results and Discussion

Diffusion coefficient of ferricyanide.—Under the limiting-current condition, a modified Levich's equation for the pure rotating disk flow can be deduced from Eq. 30 with $K = 0$ and expressed as

$$i_l = \frac{0.62048nFD_i\omega^{1/2}\nu^{1/2}Sc^{-2/3}C_{i,b}}{1 + 0.2980Sc^{-1/3} + 0.1451Sc^{-2/3} + 0.0702Sc^{-1} + 0.0352Sc^{-4/3}} \qquad [24]$$

where i_l is the limiting current density in A/cm^2. Equation 24 is similar to the one presented by Newman[31]. The

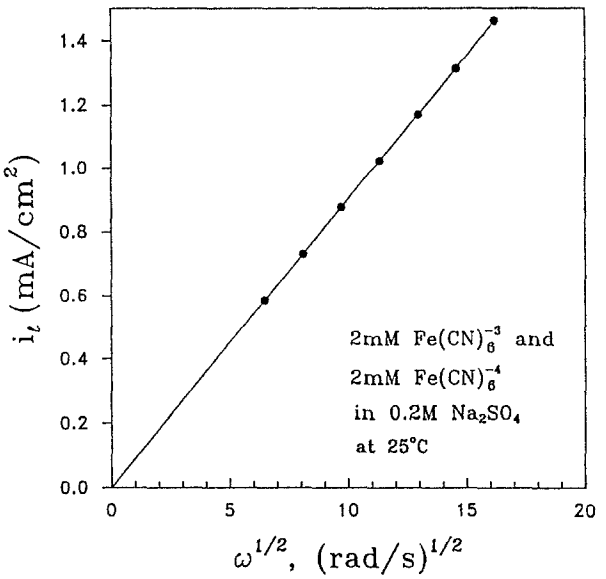

Fig. 6. Plot of i_l vs. $\omega^{-1/2}$.

above expression is much better than the Levich equation, since the latter overestimates Sh by 3% even at Sc = 1000. The diffusion coefficient can be determined from the dependence of the limiting current density i_l on the square root of the rotating speed $\omega^{1/2}$. The diffusion coefficient of ferricyanide ion was estimated by iterations according to Eq. 24 from the slope of the best fitted line of i_l *vs.* $\omega^{1/2}$, as shown in Fig. 6. The value is 6.68×10^{-6} cm^2/s, which is in good agreement with the literature values[20,34]. So the Schmidt number for ferricyanide in 0.2*M* Na_2SO_4 solution at 25°C is 1402.

Evaluation of hydrodynamic constant, k.—The radial velocity along the disk surface for a circular disk of radius r_o in a uniform flow can be expressed as[35]

$$u = \frac{2U}{\pi} \frac{r}{r_o\left[1-\left(\frac{r}{r_o}\right)^2\right]^{1/2}} \qquad [25]$$

which could be derived from the potential theory. Here, U is the free-stream velocity of the uniform flow. According to Homman axisymmetric stagnation flow, the radial velocity for axisymmetric stagnation flow is given as $u = kr$[36]. The relation is valid no matter whether the flow at the nozzle exit is laminar or turbulent[20]. So the hydrodynamic constant k is related to the velocity of the forced flow U as

$$k = \frac{2U}{\pi} \frac{1}{r_o\left[1-\left(\frac{r}{r_o}\right)^2\right]^{1/2}} \qquad [26]$$

If r/r_o is small enough, which means in the region near the center of the disk, k may be expressed as

$$k = \frac{2}{\pi r_o} U \qquad [27]$$

If the disk electrode embedded in the inert insulator is small enough, k can be evaluated from the above equation. Because the ratio of the disk electrode to the small disk used in the experiment was $r_e/r_o = 0.228/0.666 = 0.343$, it seemed more reasonable to take the average value of k from Eq. 26. The result is

$$\bar{k} = \frac{r_e}{r_o} \sin^{-1} \frac{r_e}{r_o} \times \left(\frac{2}{\pi r_o} U\right) \qquad [28]$$

For $r_e/r_o = 0.343$, $\bar{k} = 1.02 \times (2/\pi r_o U)$. Therefore, even though r_e/r_o is as large as 0.343, the difference between k and $\bar{k}$ is only 2%. In our calculation, $\bar{k}$ was used instead of k.

Mass transfer at the forced-convective rotating and stationary disk electrodes.—The dimensionless mass-transfer factors measured in this experiment are listed in Table III

Table III. Experimental data.

U (cm/s)	$\bar{k}$ (1/s)	ω (rad/s)	$\mu = \omega\sqrt{\bar{k}}$	i_l (mA/cm^2)	Sh/Sc$^{1/3}$ Exptl.	Sh/Sc$^{1/3}$ Theory
5.803	5.657	0.000	0.000	0.355	1.000	0.843
		10.472	1.851	0.386	0.750	0.680
		20.944	3.702	0.458	0.660	0.629
		31.416	5.553	0.534	0.634	0.615
		41.888	7.404	0.602	0.621	0.610
		52.360	9.256	0.666	0.616	0.607
		62.832	11.107	0.725	0.612	0.606
		94.248	16.660	0.877	0.605	0.604
9.118	8.890	0.000	0.000	0.442	0.995	0.843
		10.472	1.178	0.454	0.822	0.732
		20.944	2.356	0.499	0.702	0.658
		31.416	3.534	0.562	0.660	0.631
		41.888	4.712	0.621	0.637	0.619
		52.360	5.890	0.682	0.628	0.614
		62.832	7.068	0.737	0.621	0.610
		73.304	8.246	0.792	0.618	0.608
16.579	16.163	0.000	0.000	0.579	0.965	0.843
		10.472	0.648	0.587	0.897	0.793
		20.944	1.296	0.609	0.794	0.720
		31.416	1.944	0.640	0.722	0.675
		41.887	2.592	0.688	0.689	0.650
		62.832	3.887	0.780	0.649	0.626
		83.776	5.183	0.865	0.628	0.617
		104.720	6.479	0.962	0.627	0.612
24.868	24.245	0.000	0.000	0.704	0.958	0.843
		10.472	0.432	0.694	0.906	0.818
		26.180	1.080	0.722	0.810	0.742
		41.888	1.728	0.745	0.718	0.688
		62.832	2.592	0.822	0.672	0.650
		83.776	3.455	0.904	0.649	0.632
		104.720	4.319	0.987	0.638	0.622
		125.664	5.183	1.060	0.628	0.617
41.447	40.408	0.000	0.000	0.834	0.881	0.843
		10.472	0.259	0.826	0.857	0.833
		26.180	0.648	0.839	0.811	0.793
		41.888	1.037	0.852	0.749	0.746
		78.540	1.943	0.950	0.678	0.675
		104.720	2.592	1.023	0.648	0.650
		130.900	3.239	1.109	0.635	0.635
		167.552	4.147	1.212	0.619	0.624
62.170	60.612	0.000	0.000	0.979	0.844	0.843
		10.472	0.173	0.980	0.838	0.839
		26.180	0.432	0.987	0.815	0.818
		41.888	0.691	1.003	0.783	0.787
		78.540	1.296	1.051	0.708	0.720
		104.720	1.728	1.114	0.679	0.688
		130.900	2.160	1.170	0.653	0.665
		167.552	2.764	1.267	0.637	0.645

and plotted in Fig. 7. The complete solution (solid line) is computed by the numerical integration of the convective-diffusion equation, Eq. 18, and the approximate solution

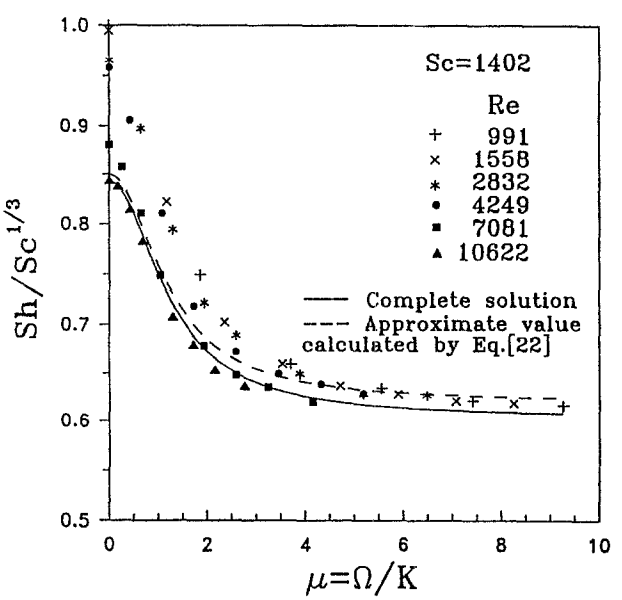

Fig. 7. Sh/Sc$^{1/3}$ vs. μ under various Reynolds numbers of the forced flow.

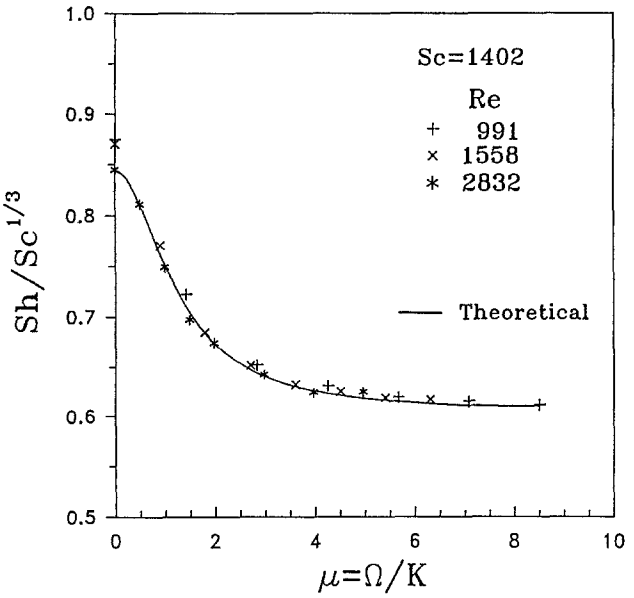

Fig. 8. $Sh/Sc^{1/3}$ *vs.* μ for laminar flow in which the velocity used to calculate $\bar{k}$ was corrected according to Eq. 29.

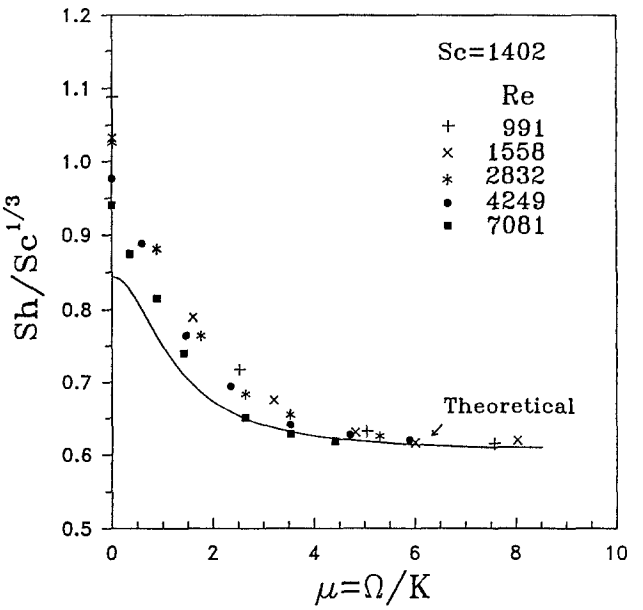

Fig. 9. $Sh/Sc^{1/3}$ *vs.* μ for various Reynolds numbers of the forced flow. The experimental data were obtained by the larger disk, r_o = 0.9 cm, and $\bar{k}$ was calculated on the basis of disk radius.

(dashed line) is calculated according to Eq. 22, which is exact for very large Schmidt numbers. By comparing the experimental data with the complete solution, it is found that there is a satisfactory agreement if the flow in the nozzle is turbulent (Re > 4000; the Reynolds number is based on the diameter of the circular nozzle, *i.e.*, Ud_n/ν). But the agreement does not seem good, if the flow in the nozzle is laminar (Re < 2100), especially when Ω/K is small. As we know, the velocity profile is parabolic in the nozzle for laminar flow. The velocity near the central line is greater than the average velocity. Therefore, the calculated hydrodynamic strength $\bar{k}$ based on the average velocity U will be smaller than that based on the actual velocity. In order to account for the deviations caused by the $\bar{k}$ values in the laminer flow region, the velocity profile in the nozzle was considered and $\bar{k}$ should be corrected as

$$U^* = 4U\int_0^{r_o} r\left[1-\left(\frac{r}{r_n}\right)^2\right]dr/r_o^2 = 1.306U \qquad [29]$$

where r_o = 0.666 cm, and U^* represents the effective free-stream velocity from the nozzle. The dimensionless mass-transfer factors after replacing U by U^* in the calculation of $\bar{k}$ is replotted and shown in Fig. 8. As can be seen in Fig. 8, the measured mass-transfer coefficients are in good accordance with the theoretical values. For turbulent flow in a smooth circular tube, the velocity profile over the cross section is much more uniform than that in laminar flow. So it is not necessary to use Eq. 29 to correct $\bar{k}$ for turbulent flow.

Figure 9 is the plot of $Sh/Sc^{1/3}$ *vs.* the relative rotating strength μ for the theoretical values and the experimental results obtained by the larger disk (r_o = 0.9 cm). The disk radius was used for calculating $\bar{k}$ and Sh. It is found that the deviations from theoretical values are more obvious than those obtained previously by the smaller disk (r_o = 0.666 cm). The discrepancy reveals the evaluation of $\bar{k}$ by use of the disk radius is inappropriate if the disk radius becomes larger than the nozzle radius. In this case, however, the disk would be supposed to have the same radius as the nozzle, and the value of $\bar{k}$ could be determined accordingly. The results with this correction are replotted in Fig. 10, and the agreement is shown to be improved. The same difficulty in estimating the hydrodynamic strength k had been encountered in the study of Chin and Tsang[21]. The electrode used in their experiments was mounted in a Plexiglas plate, the diameter of which was larger than the diameter of the nozzle. Although they presented a theoretical equation as Eq. 22 with a = 1.3119 for predicting mass-transfer rates, the experimental data were not compared with their theoretical values. Instead, the experimental data were correlated as two empirical equations. One is suitable for laminar flow, and the other for turbulent flow. We also applied our approach to determine the hydrodynamic strength k of the experimental results by Chin and Tsang[20]. The data were taken directly from their paper[20], and the results for the stationary electrode impinged by a jet are shown in Fig. 11. The mass-transfer factor $Sh/Sc^{1/3}$ is independent of the Reynolds number in the nozzle, because the Sherwood number Sh involves the mixed flow strength λ which can be related to the hydrodynamic strength of the forced flow from the nozzle. In general, the experimental data fall within 10% of the theoretical prediction, as well as their correlations could predict.

Effect of nozzle height on mass transfer.—Equation 29 is based on the assumption that the velocity distribution near the exit of the nozzle is the same as that in the feed tube. As a rule, the core length of the jet extends 4.7 to 7.7 nozzle

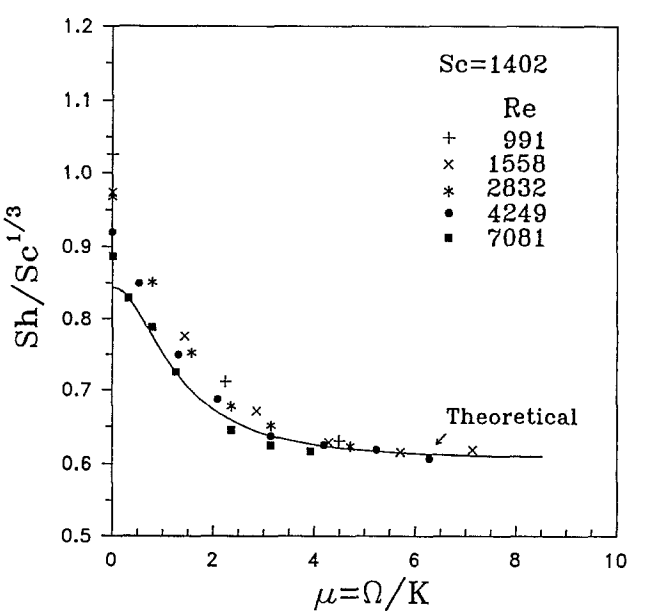

Fig. 10. $Sh/Sc^{1/3}$ *vs.* μ for various Reynolds numbers of the forced flow. The experimental data were obtained by the larger disk, r_o = 0.9 cm, and $\bar{k}$ was calculated on the basis of the nozzle radius.

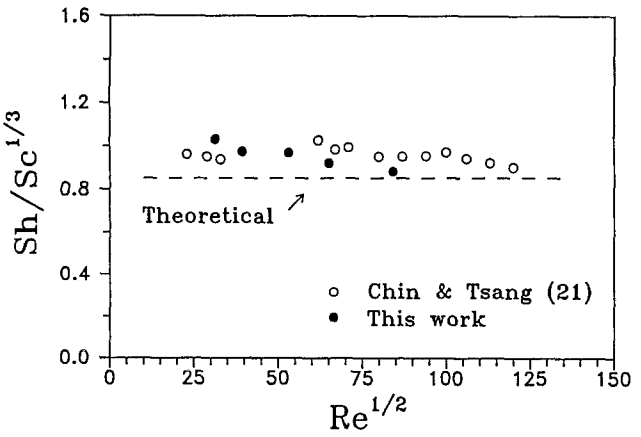

Fig. 11. Comparison between the results of this work and Chin and Tsang[20] for the stationary electrode impinged by a jet. The data in Fig. 10 are used.

diameters[37]. Thus, if the distance between the disk and the nozzle is not too far, Eq. 29 is suitable for calculating U^*. Three distances (h/d_n = 0.125, 0.9375, 1.875) were taken for measurements in our experiments, and one of the results is shown in Fig. 12. The dimensionless mass-transfer factor, $Sh/Sc^{1/3}$, for both h/d_n = 0.9375 and 1.875 was found to be almost the same. In fact, there were no differences observed over our experimental ranges of rotating speed of the disk and flow rate of the impinging jet. But in the case of h/d_n = 0.125, the mass-transfer factor was obviously higher than those measured in the other two cases. The difference became smaller as the rotating speed increased, because the mass-transfer rate for a forced-convective rotating disk was dominated by the rotating speed of the disk when the relative strength ratio of rotating speed to external convection was high. Scholtz and Trass[16] studied the effect of nozzle height on the mass-transfer rate from the impinging jet, and concluded that the mass-transfer rate was independent of nozzle height in the range of 0.5 to 12 nozzle radii. Our experimental results also confirmed their arguments. As the disk is too close to the nozzle, the flow exit for the fluid out of the nozzle becomes narrow and the boundary effect of the disk becomes more significant. The fluid accelerates rapidly in the radial direction as an outcome, of course, and the calculation of the hydrodynamic constant k becomes more difficult.

Although the theoretical analysis is based on the assumption that the external forced flow is laminar, the experimental results coincide with the theoretical prediction no matter whether the flow in the nozzle is laminar or turbulent. Indeed, turbulent flows in the nozzle are much closer to our theoretical consideration, *i.e.*, the rotating disk is in uniform forced convection, because it is well known that the velocity distribution across the nozzle is more uniform under turbulent flow. The variation of hydrodynamic constant k with radius has been considered in this study but the dsitribution of mass-transfer rates in the radial direction has not been investigated yet. For the electrode used in the experiment, the variation of the hydrodynamic constant k along the disk-electrode surface is so small that the mass-transfer distribution at the forced-convective rotating-disk electrode can be regarded as uniform.

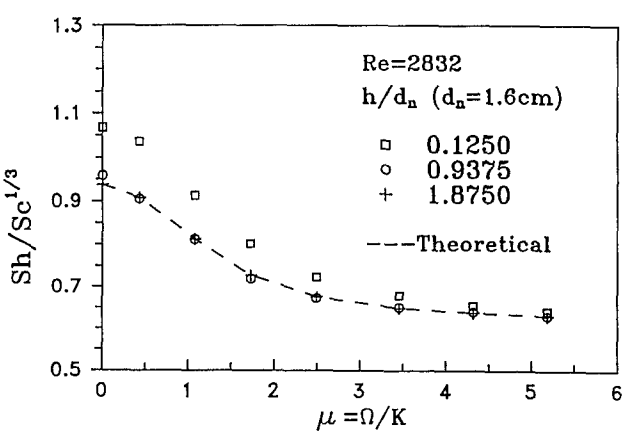

Fig. 12. $Sh/Sc^{1/3}$ vs. μ at various ratios of the nozzle-disk distance to the nozzle diameter, h/d_n.

Conclusions

The mass transfer for a rotating disk imposed by an external forced flow has been studied in this work. In addition to the theoretical analysis, the mass-transfer rates were measured by the electrochemical method. A comparison was made between the experimental and theoretical values. The corresponding mass-transfer rates were formulated from integrating the convective diffusion equation after the velocities were solved. An asymptotic expression has been obtained by taking the first few terms of the velocity profile, which is accurate down to Sc = 1. It has been found that the mass-transfer factors measured in the experiment are in good agreement with the theoretical values in the turbulent-flow region in the nozzle. For laminar flow in the nozzle, the accordance would be greatly improved if the velocity distribution in the flow is taken into consideration.

Acknowledgment

This work was supported by the National Science Council of Taiwan, China, under Contract No. NSC 81-0402-E002-02.

Manuscript submitted Nov. 18, 1991; revised manuscript received April 10, 1992.

National Taiwan University assisted in meeting the publication costs of this article.

LIST OF SYMBOLS

a	flow constant used in series expansion
b	flow constant used in series expansion
C	dimensionless flow constant
$C_{i,b}$	bulk concentration of species i, mol/cm^3
C_s	surface concentration of species i, mol/cm^3
d_n	diameter of the circular nozzle, cm
D_i	diffusion coefficient of species i, cm^2/s
F	Faraday's constant, 96,487 C/eq
F, G, H	dimensionless velocity functions in radial, angular, and axial direction, respectively
h	nozzle height, cm
i_l	limiting current density, A/cm^2
k_m	mass-transfer coefficient, mol/cm^2-s
k	hydrodynamic strength of the forced flow, 1/s
$\bar{k}$	average hydrodynamic strength of the forced flow defined in Eq. 28, 1/s
K	dimensionless parameter of the forced convection (=k/λ)
r	radial coordinate, cm
r_e	radius of the disk electrode embedded in the disk, cm
r_o	radius of the disk, cm
r_n	radius of the nozzle, cm
u	velocity component in r-direction, cm/s
U	average velocity in the nozzle exit, cm/s
U^*	effective free-stream velocity, cm/s
v	velocity component ϕ-direction, cm/s
w	velocity component in z-direction, cm/s
z	coordinate normal to disk surface, cm

Greek

Γ	gamma function
ζ	dimensionless axial distance defined in Eq. 2
Θ	dimensionless concentration (=$C_i - C_s/C_{i,b} - C_s$)
λ	mixed flow parameter (=$(k^2 + \omega^2)^{1/2}$), 1/s
μ	ratio of the rotating speed to the strength of the forced convection (=Ω/K)
ν	kinematic viscosity of fluid, cm^2/s
ω	angular velocity in ϕ-direction, rad/s
Ω	dimensionless parameter of the rotating disk flow (=ω/λ)

Dimensionless

Re	Reynolds number in the nozzle, Ud_n/ν
Sc	Schmidt number ($=\nu/D_i$)
Sh	Sherwood number ($=k_m/D_i(\lambda/\nu)^{-1/2}$)

REFERENCES

1. A. C. Riddford, *Adv. Electrochem. Electrochem. Eng.*, **4,** 47 (1966).
2. M. E. Coltrin, R. J. Kee, and G. H. Evans, *This Journal,* **136,** 819 (1989).
3. J. N. B. Livingood and P. Hrycak, *NASA TM X-2778* (1973).
4. F. Giralt and O. Trass, *Can. J. Chem. Eng.,* **53,** 505 (1975), *ibid.,* **54,** 148 (1976).
5. T. von Kármán, *Z. Angew. Math. Mech.,* **1,** 244 (1921).
6. W. G. Cochran, *Proc. Cambr. Phil. Soc.,* **30,** 365 (1934).
7. E. M. Sparrow and J. L. Gregg, *J. Heat Transfer,* **82C,** 294 (1960).
8. J. Newman, *J. Phys. Chem.,* **70,** 1327 (1966).
9. K. T. Liu and W. E. Stewart, *Int. J. Heat Mass Transfer,* **15,** 187 (1972).
10. C. L. Tien and D. T. Campbell, *J. Fluid Mechanics,* **17,** 105 (1963).
11. J. Newman and L. Hsueh, *Electrochim. Acta,* **12,** 417 (1967).
12. M. Daguenet, *Int. J. Heat Mass Transfer,* **11,** 1581 (1968).
13. F. Kreith, J. H. Taylor, and J. P. Chong, *Trans. ASME, J. Heat Transfer,* **81,** 95 (1959).
14. C. M. Mohr, Jr., and J. Newman, *This Journal,* **123,** 1687 (1976).
15. B. T. Ellison and I. Cornet, *ibid.,* **118,** 68 (1971).
16. M. T. Scholtz and O. Trass, *AIChE J.,* **16,** 82 (1970).
17. M. T. Scholtz and O. Trass, *ibid.,* **9,** 548 (1964).
18. J. Yamada and H. Matsuda, *J. Electroanal. Chem.,* **44,** 189 (1973).
19. F. Coeuret, *Chem. Eng. Sci.,* **30,** 1257 (1975).
20. D. T. Chin and C. H. Tsang, *This Journal,* **125,** 1461 (1978).
21. D. T. Chin and R. R. Chandran, *ibid.,* **128,** 1904 (1981).
22. R. C. Alkire and T. J. Chen, *This Journal,* **129,** 2424 (1982).
23. D. M. Hannah, *Br. Aero. Res. Comm. Rep. Memo.,* No. 2772 (1947).
24. H. Schlichting and E. Truckenbrodt, *J. Aero. Sci., Readers' Forum,* **18,** 639 (1951).
25. C. L. Tien and J. Tsuji, *Int. J. Heat Mass Transfer,* **7,** 247 (1964).
26. M. H. Lee, D. R. Jeng, and K. J. De Witt, *Trans. ASME, J. Heat Transfer,* **100,** 496 (1978).
27. S. S. Koong and P. L. Blackshear, *ibid.,* **87,** 442 (1965).
28. S. C. Yen and J. S. Wang, *Chem. Eng. Sci.,* In press (1991).
29. R. Caban and T. W. Chapman, *Chem. Eng. Sci.,* **36,** 849 (1981).
30. J. Newman, *J. Phys. Chem.,* **70,** 1327 (1966).
31. J. S. Newman, *Electrochemical Systems,* Prentice-Hall, Englewood Cliffs, NJ (1973).
32. W. H. Smyrl and J. Newman, *This Journal,* **118,** 1079 (1971).
33. E. Gileadi, E. Kirowa-Eisner, and J. Penciner, *Interfacial Electrochemistry—An Experimental Approach,* Addison-Wesley Publishing Co., Inc., Reading, MA (1975).
34. A. J. Arvia, S. L. Marchiano, and J. J. Podesta, *Electrochim. Acta,* **12,** 259 (1967).
35. H. Lamb, *Hydrodynamics,* Dover, New York (1945).
36. F. Homman, *ZAMN,* **16,** 153 (1936); also see H. Schlichting, *Boundary Layer Theory,* 7th ed., pp. 95-98, McGraw-Hill, Inc., New York (1979).
37. J. W. Gauntner, J. N. B. Livingood, and P. Hrycak, *NASA Tn* D5652 (1970).

Erratum

The affiliation of Dr. Chris A. Mack, the author of the Electrochemical Society Letter "New Kinetic Model for Resist Dissolution" which appeared in the April 1992 issue of the *Journal* [*This Journal*, Vol. **139** (4), pp. L35-L37 (1992)] should be FINLE Technologies, Plano, Texas 75026. FINLE Technologies assisted in meeting the publication costs of that article.